Prepared for: Brain

Title: A Predictive Epilepsy Index Based on Probabilistic Classification of Interictal Spike Waveforms

Jesse A. Pfammatter[1*], Rachel A. Bergstrom[2*], Eli P. Wallace[1], Rama K. Maganti[3], and Mathew V. Jones[1]

[1]Department of Neuroscience, University of Wisconsin, 1111 Highland Avenue, Madison, WI, 53705

[2]Department of Biology, Beloit College, 700 College Street, Beloit, WI 53511

[3]Department of Neurology, University of Wisconsin, 1685 Highland Avenue, Madison, WI 53705

*These authors contributed equally to this manuscript

Corresponding Author:

Jesse Pfammatter
5505 WIMR II
1111 Highland Ave.
Madison WI, 53705
email: pfammatter@wisc.edu

Abstract

Quantification of interictal spikes in EEG may provide insight on epilepsy disease burden, but manual quantification of spikes is time-consuming and subject to bias. We present a probability-based, automated method for the classification and quantification of interictal events, using EEG data from kainate- (KA) and saline- (SA) injected mice several weeks post-treatment. We first detected high-amplitude events, then projected event waveforms into Principal Components space and identified clusters of spike morphologies using a Gaussian Mixture Model. We calculated the odds-ratio of events from KA versus SA within each cluster, converted these values to probability scores, P(KA), and calculated an Hourly Epilepsy Index for each animal by summing the probabilities for events where the cluster P(KA) > 0.5 and dividing the resultant sum by the record duration. This Index is predictive of whether an animal received an epileptogenic treatment (i.e., KA), even if a seizure was never observed. We applied this method to an out-of-sample dataset to assess epileptiform spike morphologies in five KA animals monitored for ~1 month. The magnitude of the Index increased over time in a subset of animals and revealed changes in the prevalence of epileptiform (P(KA) > 0.5) spike morphologies. Importantly, in both data sets, animals that had electrographic seizures also had a high Index. This analysis is fast, unbiased, and provides information regarding the salience of spike morphologies for disease progression. Future refinement will allow a better understanding of the definition of interictal spikes in quantitative and unambiguous terms.

Keywords and Abbreviations

Keywords:

Temporal Lobe Epilepsy (TLE), kainate, automated event detection, mouse

Abbreviations:

EEG: electroencephalogram

KA: kainate

SA: saline

P(KA): probability of having received KA treatment

PCA: Principal Components Analysis

GMM: Gaussian Mixture Model

Introduction

The electroencephalogram (EEG) is an essential tool for monitoring seizures, diagnosing epilepsy and understanding epileptogenesis. Most EEG analysis, including the scoring of seizures and interictal epileptiform events, is carried out manually by trained scorers. Manual scoring is labor-intensive and prone to low interobserver agreement (Webber *et al.*, 1993) which often precludes fine-scale and quantitative analysis of EEG, especially for chronic (>24 hours) recordings commonly employed in clinical and research settings (Boly and Maganti, 2014; Fisher *et al.*, 2014).

Adding to the challenge of EEG analysis and diagnosis in epilepsy is a relatively low seizure frequency, often much less than one/day, making capturing confirmatory seizure events on EEG rare (White *et al.*, 2010). Thus, the identification and analysis of subclinical, interictal events such as spikes may be important for diagnosis, identification of epileptic foci and understanding the progression of epilepsy (Cascino *et al.*, 1992; Krendl *et al.*, 2008; Miller and Gotman, 2008; White *et al.*, 2010; Barkmeier *et al.*, 2012; Boly and Maganti, 2014; Avoli *et al.*, 2013; Tomlinson *et al.*, 2016). But the definition of spike-like events for subsequent manual scoring remains an area of some disagreement among clinicians (Fisher *et al.*, 2014) and researchers (Webber *et al.*, 1993; Webber and Lesser, 2017). Together with the laborious nature of manual EEG analysis, this means that the frequency of interictal spiking is not typically quantified for diagnostic purposes in the clinic, though there are special cases, and is underutilized in epilepsy research.

There are many automated approaches for detecting interictal events, including template-matching (Lodder *et al.*, 2013), non-linear energy operator (NEO) detection (

Mukhopadhyay and Ray, 1998; Malik *et al.*, 2016) wavelet filtering and line length (Bergstrom *et al.*, 2013), and neural networks (Scheuer *et al.*, 2017) among others (Wilson and Emerson, 2002). These algorithms rely in part upon a spike definition that is based on expert visual analysis and are rooted in some version of the definition by Chatrian et al 1974, where a spike is a transient that is clearly distinguishable from background activity, with a duration from 20 to 70 ms (Chatrian *et al.*, 1974; Noachtar and Schmidt, 2010; Kane *et al.*, 2017). Still, a universal ground truth definition of an interictal spike is lacking as demonstrated in many cases where interobserver agreement may be relatively low (Gerber *et al.*, 2008; Webber *et al.*, 1993). Further careful analysis of spike and spike-like event morphology is needed to refine this definition and to improve the utility of spike analysis in epilepsy.

Animal studies also demonstrate that spiking of some type can be present in both normal and epileptic brains of rodents (White *et al.*, 2010; Fisher *et al.*, 2014; Pearce *et al.*, 2014; Twele *et al.*, 2017), making it important to identify aspects of spike-like morphologies that are specifically associated with epilepsy. But differentiation of the many spike types and shapes by visual or algorithmic analysis is a difficult prospect. Rigorous differentiation and quantification of spikes in epileptic versus normal animals could elucidate patterns of activity that shed light on spike-related mechanisms in epilepsy and identification of epileptic foci while also contributing to an unbiased definition of true interictal spiking activity across models of epilepsy. Given the links between interictal spiking and disease progression in epilepsy (Goodin and Aminoff, 1984; Staley *et al.*, 2011), quantitative understanding and differentiation between

normal and epileptiform spike-like activity is essential for future progress in epilepsy research; studies in animal models are essential to this progress.

Classification of spikes based on waveform morphology is a promising approach for differentiating events that are normal versus those that are relevant to epilepsy. Indeed, spike sorting by waveform clustering has been used to tune spike-detection and quantification algorithms (Nonclercq *et al.*, 2012), to choose spike templates (Thomas *et al.*, 2016) and to identify or predict epileptic foci (Wahlberg and Lantz, 2000). A very well-studied use of waveform clustering is to distinguish individual extracellularly recorded action potential waveforms in order to identify neurons in single-unit recordings (Souza *et al.*, 2018). Several clustering approaches have been used across these applications, including K-means clustering and affinity propagation (Thomas *et al.*, 2016), graph theoretical algorithms (Wahlberg and Lantz, 2000), and Gaussian Mixture Models (GMM) (Souza *et al.*, 2018).

Here we use a novel waveform-based analysis to compare spike-like events recorded from mice treated with an epileptogenic insult (i.e., kainate, a model of temporal lobe epilepsy (Lévesque and Avoli, 2013)) with spike-like events recorded from control mice treated with saline. We identified spike-like events in both groups, then projected these waveforms into a low-dimensional (3D) space using Principal Components Analysis (PCA), and clustered these waveforms using a GMM. This allowed us to estimate the probability distributions that characterize normal versus epileptiform spike-like waveforms and to compute the probability that specific spike waveforms reflect epileptiform activity. By assigning a probability score to each event type, we provide a novel measure (the Hourly Epilepsy Index) for estimating the

128 probability that an animal is epileptic, even in the absence of observing electrographic
129 or behavioral seizures. The novel analysis thus provides rapid and unbiased insight into
130 differences among spike types in normal and epileptic animals that can be used for
131 early diagnosis of risk and serve as a biomarker of disease progression.

132 Methods

133 *Animals*

134 All use of animals in this manuscript conformed to the *Guide for the Care and*
135 *Use of Laboratory Animals* (2010) and was approved by the University of Wisconsin-
136 Madison Institutional Animal Care and Use Committee.

137 Animals (C57BL/6J background, ~5 weeks old) were received from Harlan
138 (Madison, WI) and housed in groups with rodent chow and water available *ad libitum.*
139 After ~2 weeks of acclimation, animals underwent repeated low-dose kainate (KA) or
140 saline (SA) injections (~7 weeks old) and EEG implantation and recording (~18-20
141 weeks).

142 *Epilepsy Induction*

143 During the injection process, when not handled, mice were individually housed in
144 enclosed ~150 cm^3 acrylic cubicles with opaque sides and clear front portals with holes
145 to allow air exchange, and equipped with corn cob bedding and rodent chow. Animals
146 were then randomly assigned to KA or SA treatment, ear punched or tagged for
147 identification and weighed. Mice received a series of intraperitoneal (IP) injections
148 based on the following schedule (herein referred to as “repeated low-dose kainate”).
149 Mice in the KA group first received a 10 mg/kg (5.5 mM) dose of kainate (Tocris
150 Bioscience, UK) delivered in 1x phosphate-buffered saline (PBS) prepared from PBS

151 tablets (Dot Scientific, Michigan) dissolved in deionized distilled water (DDW) and filter
152 sterilized (0.22 μm, Corning, MI). Mice continued to receive injections at 2.5-5 mg/kg
153 every 20 minutes until status epilepticus (SE) occurred (4-9 injections) (Tse *et al.*, 2014;
154 Umpierre *et al.*, 2016). Mice in the SA group received the same schedule of sterile PBS
155 injections. Mice were considered to be in SE when displaying behavioral seizures of
156 level 4-5 on the Racine Scale (Racine, 1972) for a minimum of 30 minutes. Mice usually
157 experienced SE for 90-180 minutes and were allowed to recover spontaneously. Mice
158 were treated in cohorts of ~8 at a time, with a ratio of ~2:1, KA:SA animals. The first
159 cohort of mice received alternating 5 mg/kg and 2.5 mg/kg injections after the initial 10
160 mg /kg dose, but this schedule took longer than only 5 mg/kg injections without any
161 noticeable differences in eventual efficacy or survival, so subsequent cohorts received 5
162 mg/kg injections. Across all cohorts, mortality was <10%.

163 After the injection schedule, animals were given fresh apple slices, monitored
164 until SE ceased (assessed by normal posturing), and returned to group housing. They
165 were monitored, weighed, and given 0.4 mL of sterile 1x PBS via IP injection on a daily
166 basis as necessary until their weight returned to pre-injection level. No animal injected
167 with SA ever experienced status epilepticus, lost weight, or required recovery injections
168 of 1x PBS. Mice remained in the vivarium for 7-9 weeks after injections, allowing time
169 for the development of epilepsy in KA mice. During this time some KA mice became
170 aggressive and were removed from group housing and caged individually.

171 *EEG Surgery and Recording*

172 Animals were implanted with EEG headcaps (see (Wallace *et al.*, 2015) for
173 detailed methods) at ~18-20 weeks old (~11-13 weeks post injection), allowed to

recover for 3-4 days and then recorded continuously at 256, 512, or 1024 Hz sampling rate for three days. All data not collected at 512 Hz were either resampled (1024 Hz) or linearly interpolated (256 Hz) to 512 Hz for analysis. Data were then notch filtered at 60 Hz using a Chebyshev Type II digital filter and high-pass (>0.5 Hz) filtered with a Chebyshev Type I digital filter. All analyses presented in this manuscript used a right-frontal EEG channel.

High-amplitude Event Detection

To assess the severity of epilepsy in animals injected with kainate, we developed a probability-based approach for the detection of epilepsy-related events (e.g. interictal abnormal events like EEG spikes, seizures) and the calculation of an epilepsy severity index.

Filtered EEG signals were normalized to using a variation of z-score normalization that we term Gaussian normalization. First, we fit a Gaussian distribution to the all-points histogram of each 24-hour record using the Nelder-Mead Simplex (Nelder and Mead, 1965) method as implemented by the fminsearch function in Matlab. We then normalized the 24-hour record by subtracting the mean from each point and dividing by the standard deviation of the model fit. The resultant normalization is different from the standard z-score normalization in that the mean and standard deviation components are calculated from a model estimating the Gaussian components of the EEG rather than empirically calculating the mean and standard deviation. We employed this normalization because it adjusts the data based on the normal component of the signal and is less influenced by very large and brief artifacts.

196 Using normalized EEG we detected high-amplitude, spike-like events using a
197 two-threshold strategy (Twyman and Macdonald, 1991). The final thresholds used in
198 this analysis were optimized to yield the largest predictive effect size (Fig. 1D). The start
199 of an event was triggered when the EEG signal rose 5 standard deviations above the
200 mean of the Gaussian fit. An event ended when the signal passed 1 standard deviation
201 below the mean. We then combined any events occurring within 0.2 seconds of one
202 another (end to start) into a single event (Kane *et al.*, 2017). This resulted in a list of
203 events of varying duration (98% shorter than 1s, with some representing rapid spike
204 bursts) from each animal/day EEG record. We then took two seconds of signal centered
205 on the start of each event and collated events across 72 days of recording (3-4 days
206 from each of 15 KA and 7 SA animals). This resulted in a matrix with ~33000 event
207 waveforms (1024 points each) across all treatments, recording days, and animals. We
208 chose optimal high (event start) and low (event end) threshold values after a grid search
209 to investigate high values between 3 and 8, and low values between -3 and 2 and then
210 performing a t-test to compare the number of events per hour identified in SA vs. KA
211 animals (Fig. 1D).

212 *Epileptiform Event Confirmation*

213 We compared the output of the two-threshold detection method with output from
214 another method that has been highly cited for seizure and interictal spike detection, and
215 that also performs similarly to manual human scoring (Bergstrom et al. 2013). Spikes,
216 seizures, and other abnormal epileptiform activity were detected in normalized EEG
217 according to Bergstrom et al. (2013). The baseline was determined using the whole
218 signal. The event threshold (SF value) was set at 4.0, where spikes were defined using

219 a modified amplitude of 15, and seizures were defined as events greater than one
220 second in duration. To compare the two-threshold method with that of Bergstrom et al.
221 (2013), all records were represented as logical vectors where 1 indicates the presence
222 of an event during each second of recording and 0 indicates the absence of an event.
223 Confusion matrices (Fawcett, 2006) between these vectors were used to compute true-
224 positive and false-negative rates, by provisionally assuming that Bergstrom et al. (2013)
225 detected “true” events.

226 *PCA, Clustering, and P(KA)*

227 We performed Principal Components Analysis (PCA) (Hotelling, 1933) on the
228 matrix (~33000 x 1024) of waveforms detected by the two-threshold method and
229 projected each original waveform into the space spanned by the first three Principal
230 Components (PCs, Fig. 3). In such 3D projections, each point represents a detected
231 waveform and the distance between any two points represents the difference between
232 their original waveform shapes. Three dimensions were chosen for ease of display, but
233 higher or lower dimensional projections could be used throughout this analysis in
234 principle.

235 Waveforms that are closely intertwined with epilepsy should be a) more common
236 in KA than in SA and b) similar to other waveforms in epileptic (KA) mice and different
237 from those of SA mice. Therefore, the densities of PCA-projected points for KA and SA
238 events are expected to overlap somewhat but, by examining quantitatively their overlap
239 in specific regions of PCA space, we can compute the likelihood of a waveform in any
240 region having come from a KA vs SA animal.

The resulting ensemble of points was fit with a Gaussian Mixture Model (GMM) with expectation maximization using the function fitgmdist() (McLachlan and Peel, 2005) with nine components and then clustered based on the GMM coefficients. The GMM defines a probability for every point in the space, and in this case reflects the prior probability distribution that any waveform would be detected because both KA and SA were included in the GMM fit. We then calculated the conditional probability, P(KA) that events in each cluster are related to an epileptogenic treatment by computing the ratio of KA (epileptogenic) to SA (control) events in each cluster (Odds ratio) and converting it to a probability, P (using Odds = P / (1-P)).

Hourly Epilepsy Index

Given that there is some disagreement between manual scorers, we are attempting to provide a statistical and unbiased measure of epileptiform event frequencies. We first defined epileptiform event morphologies as events with a P(KA) > 0.50, because they are more likely to be found in KA than SA animals and are therefore more relevant to epilepsy. The range of P(KA) values was rescaled from 0.5 -1.0 to 0 – 1, scaled P(KA) = (P(KA) - 0.5) * 2, to reflect the relative contribution of each event morphology to the KA-specific set. Our method is probabilistic, so it can only be interpreted as an “index” rather than an actual count of interictal events. Therefore, we define an Hourly Epilepsy Index = ∑(frequency of events in each cluster with P(KA) > 0.5 x associated scaled P(KA)).

Parameter Optimization

One tunable parameter in this analysis is the choice of how many clusters to use in modeling the data (i.e., how fine-grained should our analysis of waveform shapes

be?). To investigate this parameter, we built a set of models varying the total number of GMM clusters. Additionally, because creation of a GMM in our implementation is a stochastic process, we rebuilt each model at 25 unique random seeds (seeds = 1 through 25). In total, we generated 600 Gaussian mixture models and related cluster profiles, P(KA)s, and Hourly Epilepsy Indices. From each of these model sets we calculated: 1) the Negative Loglikelihood of the data fit to the GMM, 2) The average belongingness of each event to its assigned cluster (Cluster Belongingness, defined below), 3) the effect size between SA and KA treated animals and 4) *P* value comparing the Hourly Epilepsy Index between SA and KA treated animals. Cluster Belongingness was calculated by taking the sum of squares of the set of posterior probabilities, calculated with the posterior() function in Matlab, for each event and then averaged across all events. For each event, these posterior probabilities (as many probabilities as there are clusters) provide the likelihood of belonging to each cluster in the model and these probabilities sum to one. For example, in the case of a 2 cluster model, data point A may belong equally to each cluster $P = (0.5, 0.5)$ where its Cluster Belongingness equals 0.5. In contrast, data point A may belong much more strongly to one cluster over another $P = (0.9, 0.1)$ with a cluster belongingness of 0.82. Thus, a clustering model with poor fit will have a low value for Cluster Belongingness.

Computer Programing

All analyses, data processing, and event classification was done in Matlab (Mathworks, Natick, MA) using home-written scripts. The final version of this algorithm was executed with Matlab 2017b.

Statistical Analysis

The usage of statistical tests and procedures used to estimate model fit are indicated throughout the methods section of this manuscript. All tests and statistical applications were chosen after careful consideration of data distribution (e.g. normality) and independence. All statistical tests were two-tailed. The researchers were not blinded or randomized to the treatments given to animals, but rather treatments (KA and SA) known to cause the development of epilepsy (Tse *et al.*, 2014; Umpierre *et al.*, 2016) were used to calculate probabilistic information that went into creating the Hourly Epilepsy Index. Indeed, the design of this approach was to optimize for differences between the treatments. However, we feel that this approach is warranted and importantly, the clustering of the events morphologies was unsupervised and thus 'blinded' to the treatment from which each event originated.

Data Availability

Code for the algorithm used in this manuscript has been made publicly available at the GitHub repository github.com/jessePfammatter/detectIISs. Code for the Bergstrom *et al.* algorithm can be found at github.com/bergstromr/IISdetection. Data available upon request.

Results

EEG Recording and Event Detection

We collected three days of continuous, 24-hour EEG for 15 KA and 7 SA animals and normalized the records as described above. The two-threshold event detection algorithm identified 25681 and 5764 events in KA- and SA-treated animals, respectively

309 (Fig. 1; mean ± SD event duration for KA animals = 55 ± 148 ms; for SA animals = 169
310 ± 380 ms). The average number of events per hour detected in KA (23.3 ± 27.4) and SA
311 (11.5 ± 11.0) animals using this detection method was not significantly different (Fig.
312 1C, $P = 0.166$, $t = 1.44$, df = 19.83, two-sample T-test with unequal variances). The p-
313 value for comparison of KA and SA animals was minimized by the use of the high
314 threshold of +5 and low threshold of -1, though combinations of high thresholds of four
315 or five and low thresholds of one to -2 showed low p-values relative to all other
316 combinations (Fig 1D).

317 *High-amplitude Events are Epileptiform*

318 To confirm that the events identified by the two-threshold method include
319 epileptiform events, the normalized EEG signal was analyzed using an event detection
320 and sorting algorithm that is validated with human spike scoring (Bergstrom *et al.*,
321 2013). A comparison between events detected by the two-threshold method and spikes
322 from Bergstrom *et al.* resulted in a true positive rate (TPR) of 0.781 and a false positive
323 rate (FPR) of 0.005. Thus, our initial detection of spikes agrees reasonably well with a
324 previous method that itself agrees well with human scoring. In a comparison of the two-
325 threshold detection method to all epileptiform events (spikes, seizures, and other low-
326 amplitude, short duration abnormal) from Bergstrom *et al.* (2013), the agreement
327 between the algorithms drops precipitously (Fig 2D, TPR and FPR for all events are
328 0.038 and 0.001, respectively), suggesting that the two-threshold method is selective for
329 spike-type events and does not detect low-amplitude abnormal or some seizure-like
330 events. We illustrate specific examples of agreement (Fig 2E) and disagreement (Fig

2F) between the two detection methods, highlighting that the two-threshold detection method selects for high-amplitude spike- and seizure-like activity.

Measures Predictive of an Epileptogenic Insult.

Events from KA- and SA-treated animals were projected into Principal Components space (Fig. 3A, first three PCs shown). We used the first three PC (76.7% of the overall variance) and clustered the data into nine groups using a GMM (Fig. 3B). The probability, P(KA), that a cluster morphology is relevant to epilepsy is equal to the probability of that morphology being found in KA but not SA records and was calculated as the odds ratio of the number of KA to SA events for each cluster. The P(KA) for four of nine clusters is above 0.5 (Fig 3C, range 0.73 – 0.99), indicating that event morphologies in these clusters may be specific to the KA treatment and thus related to epilepsy. On average, KA animals exhibit a significantly higher average Hourly Epilepsy Index than do SA animals (11.6 ± 14.6 for KA, 3.0 ± 2.0 for SA; $P = 0.039$, $t = 2.26$, df = 15.04, two-sample t-test with unequal variances). Two of 15 KA animals displayed electrographic seizure activity in at least one recording (Fig 3D, magenta filled circles); the average Hourly Epilepsy Index for these animals falls above the 75th percentile (top line of box plot) of the SA hourly index. We found that there was a broad spread of Hourly Epilepsy Indices across the 17 KA mice, where eight KA mice had Hourly Epilepsy Indices similar to SA mice and 9 KA mice had Hourly Epilepsy Indices above the 95% confidence interval of the SA Index (95% confidence interval for SA = 1.14 - 4.47). This interesting result is in line with published reports of varying sensitivity to systemic KA injection in epileptogenesis (Tse *et al.*, 2014; Umpierre *et al.*, 2016).

Optimization of the Clustering Algorithm

To determine the optimum number of clusters to differentiate between KA- and SA-specific spike morphologies, we calculated 600 repetitions of the Gaussian Mixture Model used to cluster events at each unique value of 2 to 25 clusters and random seeds set from 1 to 25. The Negative Loglikelihood (Fig. 4A) approaches an asymptote around eight to ten clusters, suggesting the reasonable model fit in this range. Cluster Belongingness (Fig. 4B) decreases across the simulation range with no clear inflection point (i.e. elbow) in the data to indicate diminishing returns of increasing cluster number. Effect size and p-value for the Hourly Epilepsy Index (Fig 4C and D) models indicate that the effect size and the p-value reach an asymptote in a range similar to that indicated by the Negative Loglikelihood results. Here, we have a fuzzy problem in terms of cluster selection. We selected nine clusters for our purposes and discuss cluster selection in depth in the discussion section.

Cluster Morphologies Match Published Characteristics of Interictal Spikes

We performed a preliminary waveform shape analysis by plotting individual event duration vs amplitude for each cluster. In clusters where P(KA) > 0.5 (clusters one through four, Fig. 5A) many events from KA-treated animals have a higher amplitude than do events from the same cluster found in SA-treated animals. The majority (92%) of events in these clusters for both treatment groups are shorter than 200 ms, consistent with published spike definitions. This trend is not as distinct in clusters five through nine, where P(KA) < 0.5. Further inspection of events in clusters one through four reveals that the morphologies of these event types are more classically “spikey” (short-duration events with sharp waveforms) than are events found in the remaining clusters. Finally, the majority of the events identified in KA animals (88%) were found in

377 clusters one through four, whereas events in SA animals were equally distributed
378 among the clusters with P(KA) above (49%) and below 0.5. The average number of
379 events per hour for each cluster in SA and KA shows separation between event
380 frequency in clusters one through four but not clusters five through nine (Fig. 5B, p-
381 values reported on each graph).

382 *Analysis of Out-of-Sample Data Supports the Methodology*

383 We applied the clustering approach to events detected in a novel dataset of
384 longitudinal recordings from 5 KA-treated animals (Fig 6A - D, recorded on days 30 – 34
385 and 44 – 51 post-KA). The longitudinal data were projected into the same PC space as
386 the SA and KA dataset from Fig 3A and clustered according to the same parameters as
387 Fig 3 (Fig. 6A, B). All but one animal (Animal E) experienced similar, but not identical,
388 increases over time in total event rate (average for all events per hour, Fig 6C) and
389 Hourly Epilepsy Index (clusters one through four, Fig. 6D). Electrographic seizures were
390 only detected in one animal (Animal B) at days 44 and 45; this animal displayed a trend
391 toward increasing event rate and Hourly Epilepsy Index (Fig 6C-E, magenta-filled
392 circles).

393 Discussion

394 Interictal spikes are a hallmark of the epileptic brain (Fisher *et al.*, 2014). Yet the
395 definition of an interictal spike remains somewhat nebulous, potentially biasing spike-
396 detection strategies and algorithms. Previous analyses of spikes in kainate and other
397 models of epilepsy have relied upon scoring of spikes and other interictal events to
398 differentiate between KA-treated and control animals, where more spikes are observed
399 in epileptic than in control animals (White *et al.*, 2010; Bergstrom *et al.*, 2013). In these

400 studies, control animals also exhibit spike-type events in the EEG; however, given that
401 control (and many KA animals) animals do not proceed to have seizures, it is probable
402 that some spikes arise by a non-epileptic mechanism, including spike-like events in
403 normal brain (e.g., sharp wave ripples (Fisher *et al.*, 2014), electrographic noise,
404 artifact, or damage associated with electrode implantation. That non-epileptiform spikes
405 may also be present in both normal and kainate-treated animals further complicates the
406 quantification of interictal spikes and thus the interpretation of nonconvulsive EEG
407 events in epilepsy and epileptogenesis.

408 Here we present a novel automated algorithm for probability-based differentiation
409 of epileptiform versus non-epileptiform spike and interictal EEG event morphologies in
410 the kainate model of TLE. Our algorithm detects interictal events and weights them in
411 an Hourly Epilepsy Index based on the likelihood that they are, indeed, relevant to
412 epilepsy (i.e., related to an epileptogenic insult (Lévesque and Avoli, 2013)). Interictal
413 events and seizures projected into PC space were clustered using a Gaussian Mixture
414 Model. We used the probability P(KA) that an event cluster was KA-specific to calculate
415 an Hourly Epilepsy Index as a weighted average of the number of events with a P(KA) >
416 0.5. This value successfully estimates the probability that a subject had received an
417 epileptogenic insult, in this case a KA injection. This algorithm can, in principle, be
418 generally applied to chronic EEG recordings from either experimental animals or human
419 patients, if a control data set is available for comparison. It can also provide rapid and
420 quantitative scoring of interictal events to predict the likelihood that a subject is at risk
421 for developing epilepsy even in the absence of observing electrographic or behavioral
422 seizures.

High-amplitude Event Detection is an Inclusive Starting Point

Our approach to event detection using a two-threshold algorithm selected events of high amplitude compared to background signal, but did not, at the outset, impose limitations on event duration or morphology. This method is therefore intentionally inclusive of spike and other high-amplitude, non-spike-type events that may be physiologically relevant to epilepsy. Upon visual inspection of the signal and in comparison to a validated seizure- and spike-detection algorithm, we found that this method preferentially detects spike-type and seizure-like activity in the EEG signal (Figs 1 and 2), as well as other event morphologies, including artifact (Fig 3, cluster 8). That our detection method primarily selects for high-amplitude events does not negate the possibility that low-amplitude interictal events are relevant to epilepsy and epileptogenesis. Detection and analysis of low amplitude epileptiform events is an area for further inquiry (Bergstrom *et al.*, 2013).

Selecting the Appropriate Number of Clusters Is Flexible and Application Dependent

We built on prior clustering approaches for EEG by considering how spike sorting may elucidate spike morphologies relevant to epilepsy and to differentiate these morphologies from non-epileptiform spike-like events observed in normal rodent brains (White *et al.*, 2010; Fisher *et al.*, 2014). The high-amplitude events identified in records from SA- and KA-treated animals were projected into PCA space and then clustered using a GMM with expectation maximization. Similar to spike sorting in extracellular recordings (Souza *et al.*, 2018), we found that the GMM provided a strong fit for the clustering of high-amplitude events in our dataset.

Nine clusters provided adequate separation between SA and KA-treated animals, though our analyses also found that this is, indeed, a fuzzy problem with many different options for cluster number selection depending on the features to be extracted. Spike morphology in extracellular recording is reflective of the geometry and physiological properties of individual neurons. Spike morphology in EEG may be reflective of a number of different parameters, including the underlying pathology of the spike, the spike location, the recording montage/referencing, individual patient and recording characteristics, and other features. Defining the number of clusters therefore requires careful consideration to prevent over- or under-estimation of the true number of spike morphologies.

We found that Cluster Belongingness and p-values for the separation between KA vs non-KA event morphologies improve as the number of clusters increase. However, very higher cluster numbers may be partitioning spike morphologies (clusters) based on individual animal or recording characteristics, rather than differentiating between KA and non-KA events. Selecting a smaller number (e.g. three rather than nine) of clusters for analysis does not provide statistically significant separation between KA and SA animals, so it is important to consider the tradeoffs in increasing and decreasing the cluster number for analysis (Figure 4). Through modeling using many different cluster numbers (from two to 25), we find that there is no clear “elbow” in the Negative Loglikelihood or Cluster Belongingness scores across our simulations. This indicates that there is not a hard and fast cluster number for this analysis. Still, we found that the p-value and effect size for the epilepsy index, and the Negative Loglikelihood values seemingly approached an asymptote by nine clusters (i.e. no major

469 improvements at higher cluster numbers). Thus, we selected nine clusters for our
470 analysis because it effectively separated KA from SA events while minimizing animal-
471 specific effects.

472 We further explored event morphologies of individual clusters by specifically
473 focusing on event amplitude and duration (Fig 5), as instructed by the descriptive spike
474 definition of Chatrian *et al.* (1974). Events with a P(KA) > 0.5 (clusters 1-4, more likely to
475 be found in KA than SA animals) exist within a space consistent with general definitions
476 of spikes, that is events with high amplitude and short duration (the far lower left portion
477 of the graphs in Fig 5A). As the P(KA) drops below 0.5 (clusters 5 through 9), the events
478 begin to shift toward longer, lower-amplitude characteristics. It must be noted, however,
479 that there is not a sharp demarcation in the amplitude and duration characteristics of
480 spikes above and below the cutoff of P(KA) = 0.5.

481 In applying this analysis to other models of epilepsy, we see two major
482 approaches to selecting an appropriate number of clusters, dependent upon the end
483 goal of the analysis. One approach, similar to the approach that we have taken, is to
484 identify the minimum number of clusters that provide significant separation between
485 experimental conditions or a minimum cluster number that yield clusters of visually
486 similar morphologies. A benefit to this approach would include the differentiation of
487 noise and artifact from real epileptiform activity, as we see in cluster eight (Fig 3).
488 Quantification of events could thus proceed relatively noise-free. This is similar to but
489 more specific than an approach taken by (Nonclercq *et al.*, 2012), where spike
490 morphologies in clusters that comprise less than 5% of the total spike count are
491 removed from analysis. The considerations for a fine-scaled epilepsy index are different

492 than this first approach, and would instead select a larger number of clusters for a
493 higher-resolution model of epilepsy. Care must be taken, however, not to parcellate the
494 data too far, resulting in over-fitting of the model.

495 *The Hourly Epilepsy Index: What it is, What it is Not*

496 We have introduced an Hourly Epilepsy Index as a summary descriptive variable
497 of the likelihood of epilepsy in an individual animal, calculated as an average hourly
498 event rate weighted based on the probability that an event morphology is found in KA-
499 but not SA-treated animals. Given that kainate injection is but one model of epilepsy, we
500 cannot yet claim that this is a true model that is applicable to all epilepsy models or
501 etiologies. However, this index does begin to address some of the challenges of rodent
502 models of epilepsy, namely that not all mice that receive KA-treatment will go on to
503 develop epilepsy (Lévesque and Avoli, 2013) and low seizure frequency may make it
504 difficult to identify all epileptic mice, by providing relevant probability-based estimates of
505 likelihood of an animal being epileptic.

506 There are several features of the Hourly Epilepsy Index that indicate that this
507 may be a valuable model by which to analyze EEG data in epilepsy studies. At its
508 simplest level, the Hourly Epilepsy Index provides a more robust separation between
509 KA and SA animals than does raw event count (Fig 1C vs Fig 3D) by excluding events
510 that are not likely to be epileptiform (events where $P(KA) < 0.5$) and weighting the
511 remaining events (where $P(KA) > 0.5$) according to the probability that they are, indeed,
512 epileptiform. The relevance of this new metric is further supported by data that reveals
513 that the Hourly Epilepsy Index is significantly higher for the few KA animals with
514 electrographic seizures than the average epilepsy index of SA-treated animals (fig 3D).

515 In further confirmation of this, we did not observe electrographic seizure activity in SA
516 animals or KA-treated animals that fall within the 95% CI range of the Hourly Epilepsy
517 Index for SA animals. However, these data do not fully confirm that all animals
518 displaying a high Hourly Epilepsy Index have electrographic or behavioral seizures;
519 further studies are required to confirm epilepsy.

520 Cluster one (Fig 3c, 5a) is of particular interest in considering the power of spike
521 sorting by clustering for epilepsy analysis. These events are relatively infrequent across
522 records, but are highly correlated with KA treatment (P(KA) = 0.99) and are very rare in
523 SA animals. Visual inspection of these events confirms that they are, indeed, spike-like,
524 fitting into a more classical definition of an interictal spike (Chatrian *et al.*, 1974).
525 Because these event types are almost exclusively seen in records from KA-treated
526 animals, they are weighted more strongly in the epilepsy index than are events from
527 cluster four, which show features of spiking (high amplitude, fast duration) but may also
528 cause an expert scorer to pause on their definitive identity as an interictal spike.

529 The Hourly Epilepsy Index is not without caveats, however. Kainate is a widely-
530 used model of TLE and epileptogenesis (Lévesque and Avoli, 2013), but it is only one of
531 many models. Other models, including pilocarpine, traumatic brain injury (TBI), genetic
532 or viral models of epilepsy, and kindling, rely upon different molecular mechanisms of
533 seizure induction and may therefore produce interictal events of different morphologies.
534 Ultimately, this approach may be used to produce a library of spike templates across
535 epilepsy models to further expand and refine the working definition of an interictal spike.

536 *Conclusion*

Clustering of interictal spike provides insight into event morphologies relevant to epilepsy and epileptogenesis. Using this clustering method, we isolated epilepsy-like event morphologies that were then quantified to determine the probability that a particular animal is at risk for epilepsy or not, a variable which we have called the Hourly Epilepsy Index. This probabilistic classification method for interictal event waveforms provides a biomarker for risk and development of epilepsy, even in the absence of observing electrographic or behavioral seizures. Finally, by distinguishing spike morphologies that are preferentially present in the epileptic condition, we contribute to an unbiased understanding of the definition of interictal spiking and interictal spike morphologies, as compared with spike-like events present in the nonepileptic brain.

Funding: RO1 NS075366 (MVJ), DOD PR161864 (RKM)

548 **Figure Legends**

549 **Figure 1. Event detection by two-threshold approach.** Sample traces of events
550 identified (red) using the two-threshold method (high threshold = 5 SD above Gaussian
551 mean, low threshold = 1 SD below mean) in (A) SA- and (B) KA-injected animals. Each
552 row in A and B shows an expanded view (indicated by the blue lines) of the signal
553 directly above. (C) Average number of events per hour detected in SA (black) versus
554 KA (red) animals (P = 0.166, t = 1.44 , df = 19.83, two-sample T-test with unequal
555 variances). Circles represent the average number of events per hour for each animal
556 over 3 days of recording. Closed circles represent animals that were recorded having an
557 electrographic seizure. (D) P-values comparing the average number of events per hour
558 in SA and KA animals across a set of high and low thresholds; the p-value is minimized
559 at 5 and -1. The center mark of the box and whisker plot represents the median, while
560 the lower and upper bounds of the box represent the 25th and 75th quartiles,
561 respectively; the whiskers extend to the most extreme data points or 1.5x the
562 interquartile range.

563 **Figure 2. Interictal events correspond to epileptiform activity.** We compared events
564 from the two-threshold crossing method to events detected by a validated event
565 detection and classification algorithm (Bergstrom *et al.*, 2013). Second-by-second,
566 animal-specific (SA = black, KA = red) event classification agreement (True positive
567 rate, TPR) and the rate of detection of additional events not identified in the validated
568 method (Additional events, false positive rate, FPR) for spike-type events only (A) and
569 all event types (seizures, spikes, and other low-amplitude abnormal and epileptiform
570 events, (B), with corresponding confusion matrices (spikes only C, all events D). True

positives are events detected by both the validated algorithm and the two-threshold crossing method. (E) Sample true positive events for each event type, where gray is the original EEG trace, green is two-threshold detection output, and black is Bergstrom *et al*., 2013 detection output. (F) Sample events for each detection method that were not detected by the other method.

Figure 3. Event sorting by clustering and Hourly Epilepsy Index. (A) Events detected with the two-threshold crossing method, from all animals and records, and projected into Principal Components space (first three PCs shown, red = KA, black = SA). (B) Events in A clustered into 9 groups using a GMM with Expectation Maximization. The upper inset shows a rotated and expanded view of the same plot, allowing a view of cluster 5 (embedded within cluster 6, which is set to 10% transparency for visualization). (C) P(KA) for each cluster identified in B calculated from the relative proportion of KA to SA events, presented in descending order with examples of events. (D) The average Hourly Epilepsy Index (15 KA, 7 SA animals) is much higher for animals treated with KA ($P = 0.039$, $t = 2.26$, df = 15.04, two-sample T-test with unequal variances). The center mark of the box and whisker plot represents the median, while the lower and upper bounds of the box represent the 25th and 75th quartiles, respectively; the whiskers extend to the most extreme data points or 1.5x the interquartile range.

Figure 4. Selecting an appropriate number of clusters. We repeatedly generated a set of models (n = 25, random seeds set from 1:25) specifying a range of 2 to 25 clusters (totaling 600 models) and calculated the (A) Negative Loglikelihood, (B) Cluster Belongingness, the (C) Effect size and (D) *P* value of the Hourly KA Index comparing KA to SA treated animals (calculated using only events where P(KA) > 0.5). These values

offer guidelines for model selection via ‘elbows’ in the data which are indicative of diminishing returns in model fit. It does not appear that there is a clear best value for clustering these data into discrete groups. Therefore, the cluster number must be selected and evaluated based on the goal of the cluster analysis.

Figure 5. Characterization of individual clusters and contribution to total event count. (A) Graphical distribution of each cluster’s events in EEG amplitude (x-axis) by event duration (y-axis, time (s)) for events belonging to both KA (red) and SA (black). Example events from each cluster type are displayed in the upper right corner of each plot. For improved visualization of the majority of data, we have set the axis to exclude a small amount of the most extreme data points (most notably from cluster 7). (B) The average number of events per hour within each cluster for SA (black) and KA (red) animals. P-values indicate the results of t-tests between KA and SA for each cluster of waveform shapes.

Figure 6. Detection and categorization of interictal events in longitudinal data. We applied our detection and categorization algorithm to longitudinal EEG records (recorded days 30 – 34 and 44 – 51 post-KA) from 5 KA mice. (A) Events identified from these 5 animals (purple circles) projected into PCs with data from Figure 3 (black circles, SA and KA data). (B) Clustering of these new data points using the same GMM coefficients and clustering parameters used in Figure 3 (cluster colors correspond to those throughout manuscript). The upper inset shows a rotated and expanded view of the same plot, allowing a view of cluster 5 (embedded within cluster 6, which is set to 10% transparency for visualization). (C) Events per hour as detected by the two-threshold method in each of the 5 KA animals over time. (D) Hourly KA Index for longitudinal data set. E) Average

events per hour as detected by the two-threshold method within each cluster group. In panels C-E, records with electrographic seizures are shown as filled in circles. An example seizure is shown in the inset of panel D.

Figure 1

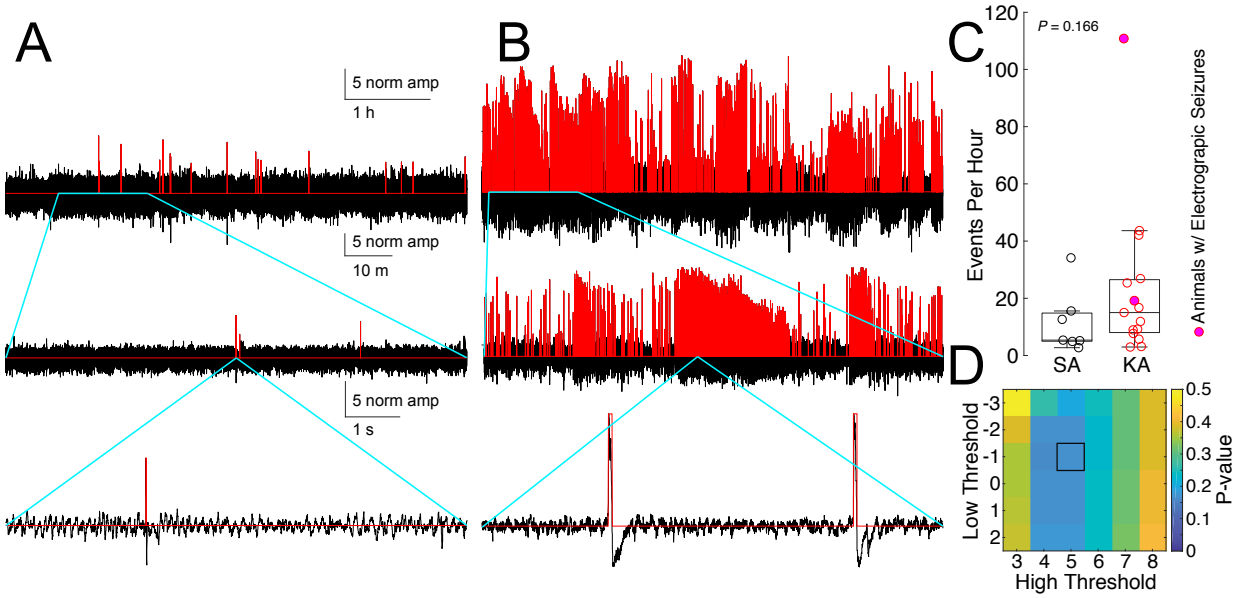
A
B
C
D
5 norm amp
1 h
5 norm amp
10 m
5 norm amp
1 s
P = 0.166
Events Per Hour
Animals w/ Electrograpic Seizures
SA
KA
Low Threshold
High Threshold
P-value

Figure 2

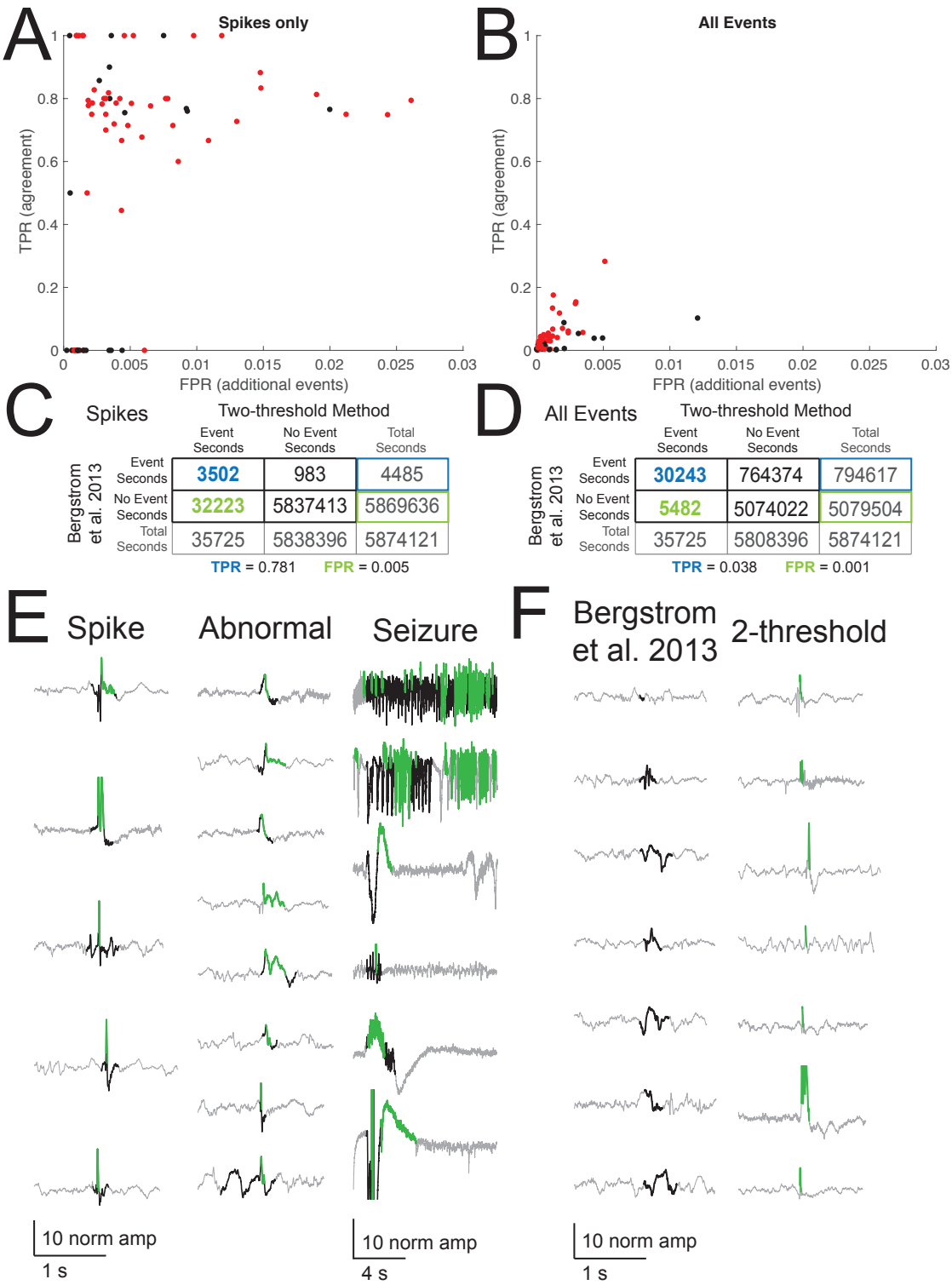
A
Spikes only
TPR (agreement)
FPR (additional events)
B
All Events
TPR (agreement)
FPR (additional events)
C
Spikes
Two-threshold Method
Bergstrom et al. 2013
Event Seconds
No Event Seconds
Total Seconds
3502
983
4485
32223
5837413
5869636
35725
5838396
5874121
TPR = 0.781
FPR = 0.005
D
All Events
Two-threshold Method
Bergstrom et al. 2013
Event Seconds
No Event Seconds
Total Seconds
30243
764374
794617
5482
5074022
5079504
35725
5808396
5874121
TPR = 0.038
FPR = 0.001
E
Spike
Abnormal
Seizure
10 norm amp
1 s
10 norm amp
4 s
F
Bergstrom et al. 2013
2-threshold
10 norm amp
1 s

Figure 3

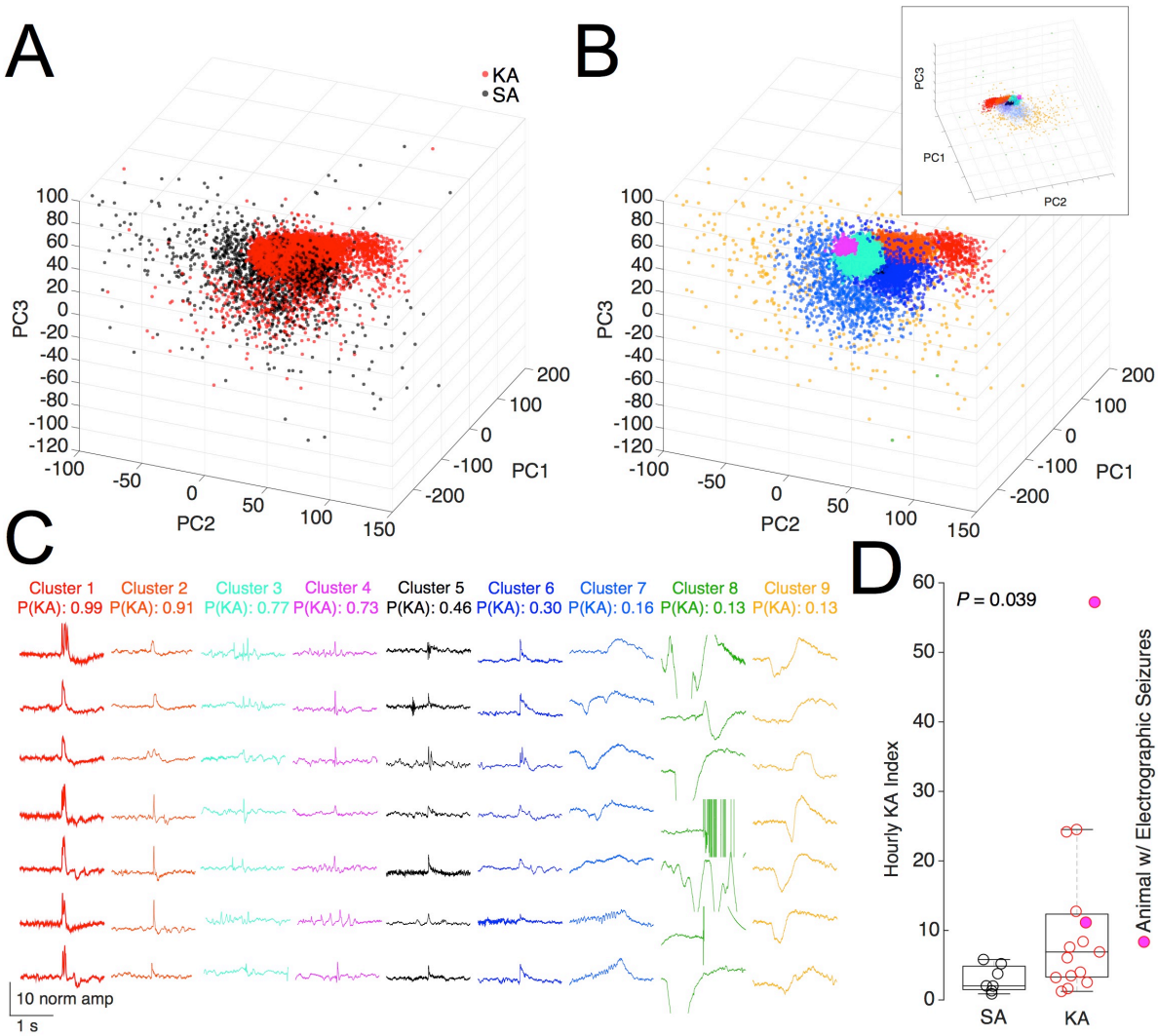
A
KA
SA
PC3
PC2
PC1
B
PC3
PC1
PC2
C
Cluster 1 P(KA): 0.99
Cluster 2 P(KA): 0.91
Cluster 3 P(KA): 0.77
Cluster 4 P(KA): 0.73
Cluster 5 P(KA): 0.46
Cluster 6 P(KA): 0.30
Cluster 7 P(KA): 0.16
Cluster 8 P(KA): 0.13
Cluster 9 P(KA): 0.13
10 norm amp
1 s
D
P = 0.039
Hourly KA Index
SA
KA
Animal w/ Electrographic Seizures

Figure 4

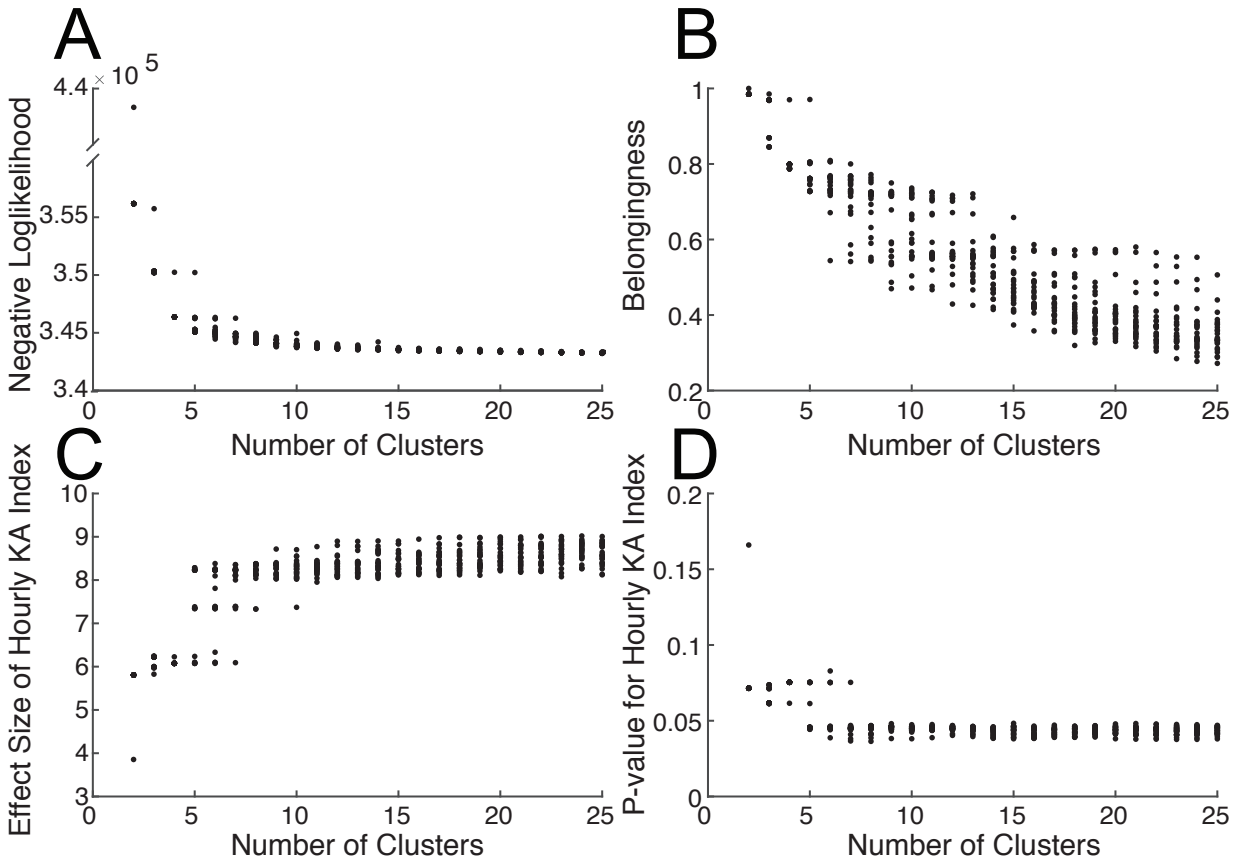
A
B
C
D
Negative Loglikelihood
Belongingness
Effect Size of Hourly KA Index
P-value for Hourly KA Index
Number of Clusters
Number of Clusters
Number of Clusters
Number of Clusters
× 10 5
4.4
3.55
3.5
3.45
3.4
1
0.8
0.6
0.4
0.2
10
9
8
7
6
5
4
3
0.2
0.15
0.1
0.05
0
0
5
10
15
20
25

Figure 5

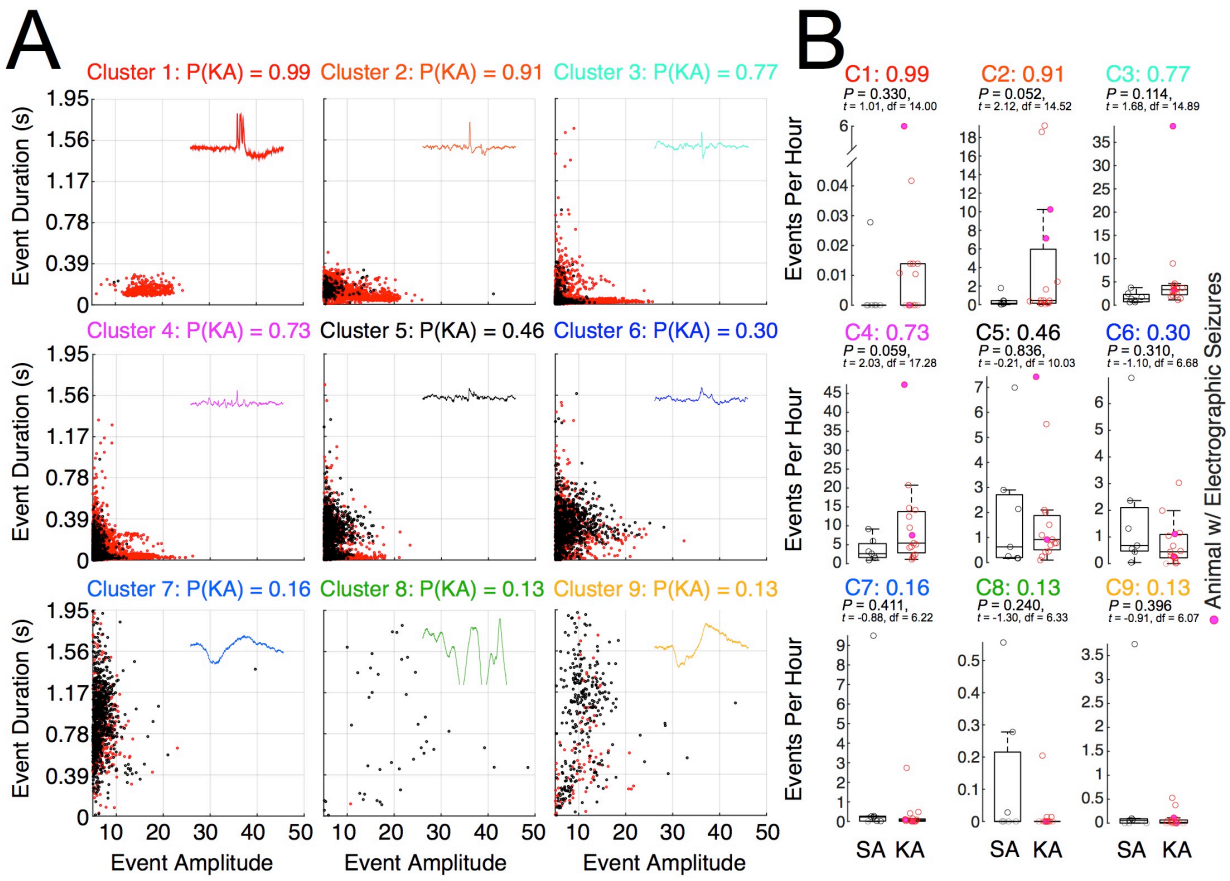
A
Cluster 1: P(KA) = 0.99
Cluster 2: P(KA) = 0.91
Cluster 3: P(KA) = 0.77
Cluster 4: P(KA) = 0.73
Cluster 5: P(KA) = 0.46
Cluster 6: P(KA) = 0.30
Cluster 7: P(KA) = 0.16
Cluster 8: P(KA) = 0.13
Cluster 9: P(KA) = 0.13
Event Duration (s)
Event Amplitude
B
C1: 0.99
P = 0.330, t = 1.01, df = 14.00
C2: 0.91
P = 0.052, t = 2.12, df = 14.52
C3: 0.77
P = 0.114, t = 1.68, df = 14.89
C4: 0.73
P = 0.059, t = 2.03, df = 17.28
C5: 0.46
P = 0.836, t = -0.21, df = 10.03
C6: 0.30
P = 0.310, t = -1.10, df = 6.68
C7: 0.16
P = 0.411, t = -0.88, df = 6.22
C8: 0.13
P = 0.240, t = -1.30, df = 6.33
C9: 0.13
P = 0.396 t = -0.91, df = 6.07
Events Per Hour
SA KA
Animal w/ Electrographic Seizures

Figure 6

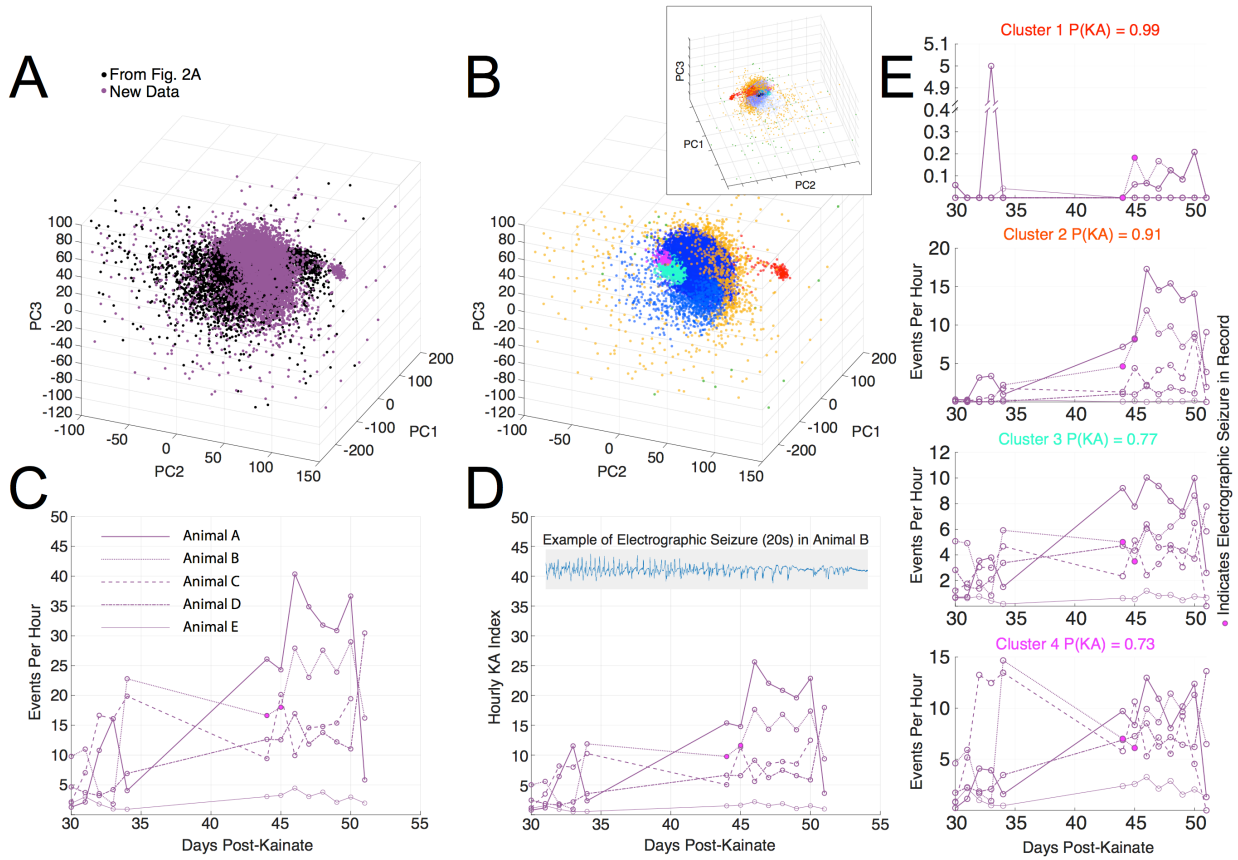
A
From Fig. 2A
New Data
PC3
PC2
PC1
B
C
Animal A
Animal B
Animal C
Animal D
Animal E
Events Per Hour
Days Post-Kainate
D
Example of Electrographic Seizure (20s) in Animal B
Hourly KA Index
E
Cluster 1 P(KA) = 0.99
Cluster 2 P(KA) = 0.91
Cluster 3 P(KA) = 0.77
Cluster 4 P(KA) = 0.73
Indicates Electrographic Seizure in Record

632 **References**

633 Avoli M, de Curtis M, Köhling R. Does interictal synchronization influence ictogenesis?
634 Neuropharmacology 2013; 69: 37–44.

635 Barkmeier DT, Senador D, Leclercq K, Pai D, Hua J, Boutros NN, et al. Electrical,
636 molecular and behavioral effects of interictal spiking in the rat. Neurobiol Dis. 2012; 47:
637 92–101.

638 Bergstrom RA, Choi JH, Manduca A, Shin H-S, Worrell GA, Howe CL. Automated
639 identification of multiple seizure-related and interictal epileptiform event types in the
640 EEG of mice. Sci Rep 2013; 3: 1483.

641 Boly M, Maganti R. Monitoring epilepsy in the intensive care unit: Current state of facts
642 and potential interest of high density EEG. Brain Injury 2014; 28: 1151–1155.

643 Cascino GD, Kelly PJ, Sharbrough FW, Hulihan JF, Hirschorn KA, Trenerry MR. Long-
644 term follow-up of stereotactic lesionectomy in partial epilepsy: predictive factors and
645 electroencephalographic results. Epilepsia 1992; 33: 639–644.

646 Chatrian GE, Bergamini L, Dondey M, Klass DW, Lennox Buchthal M, Petersen I. A
647 glossary of terms most commonly used by clinical electroencephalographers.
648 Electroenceph Clin Neurophysiol 1974; 37: 538–548.

649 Fawcett T. An introduction to ROC analysis. Pattern Recognition Letters 2006; 27: 861–
650 874.

651 Fisher RS, Scharfman HE, deCurtis M. How can we identify ictal and interictal abnormal
652 activity? Adv Exp Med Biol 2014; 813: 3–23.

653 Gerber PA, Chapman KE, Chung SS, Drees C, Maganti RK, Ng Y-T, et al. Interobserver
654 agreement in the interpretation of EEG patterns in critically ill adults. J Clin Neurophysiol
655 2008; 25: 241–249.

656 Goodin DS, Aminoff MJ. Does the interictal EEG have a role in the diagnosis of
657 epilepsy? Lancet 1984; 1: 837–839.

658 Hotelling H. Analysis of a complex of statistical variables into principal components. J
659 Educ Psychol 1933; 24: 417–441.

660 Kane N, Acharya J, Benickzy S, Caboclo L, Finnigan S, Kaplan PW, et al. A revised
661 glossary of terms most commonly used by clinical electroencephalographers and
662 updated proposal for the report format of the EEG findings. Revision 2017. Clinical
663 Neurophysiology Practice 2017; 2: 170–185.

664 Krendl R, Lurger S, Baumgartner C. Absolute spike frequency predicts surgical outcome
665 in TLE with unilateral hippocampal atrophy. Neurology 2008; 71: 413–418.

Lévesque M, Avoli M. The kainic acid model of temporal lobe epilepsy. Neurosci Biobehav Rev 2013; 37: 2887–2899.

Lodder SS, Askamp J, van Putten MJAM. Inter-ictal spike detection using a database of smart templates. Clin Neurophysiol 2013; 124: 2328–2335.

Malik MH, Saeed M, Kamboh AM. Automatic threshold optimization in nonlinear energy operator based spike detection. IEEE; 2016. p. 774–777.

McLachlan G, Peel D. Finite Mixture Models. Hoboken, NJ, USA: John Wiley & Sons, Inc; 2005.

Miller JW, Gotman J. The meaning of interictal spikes in temporal lobe epilepsy: Should we count them? Neurology 2008; 71: 392–393.

Mukhopadhyay S, Ray GC. A new interpretation of nonlinear energy operator and its efficacy in spike detection. IEEE Trans Biomed Eng 1998; 45: 180–187.

National Research Council. Guide for the Care and Use of Laboratory Animals. National Academics Press. 2010

Nelder JA, Mead R. A Simplex Method for Function Minimization. Computer J 1965; 7: 308–313.

Noachtar S, Schmidt D. Introduction. Epilepsy Behav 2010; 19: 95–95.

Nonclercq A, Foulon M, Verheulpen D, De Cock C, Buzatu M, Mathys P, et al. Cluster-based spike detection algorithm adapts to interpatient and intrapatient variation in spike morphology. J Neurosci Meth 2012; 210: 259–265.

Pearce PS, Friedman D, LaFrancois JJ, Iyengar SS, Fenton AA, MacLusky NJ, et al. Spike–wave discharges in adult Sprague–Dawley rats and their implications for animal models of temporal lobe epilepsy. Epilepsy Behav 2014; 32: 121–131.

Racine RJ. Modification of seizure activity by electrical stimulation. II. Motor seizure. Electroencephalogr Clin Neurophysiol 1972; 32: 281–294.

Scheuer ML, Bagic A, Wilson SB. Spike detection: Inter-reader agreement and a statistical Turing test on a large data set. Clin Neurophysiol 2017; 128: 243–250.

Souza BC, Lopes-dos-Santos V, Bacelo J, Tort AB. Spike sorting with Gaussian mixture models. bioRxiv 2018: 248864.

Staley KJ, White A, Dudek FE. Interictal spikes: Harbingers or causes of epilepsy? Neurosci Lett 2011; 497: 247–250.

697 Thomas J, Jin J, Dauwels J, Cash SS, Westover MB. Clustering of Intericatal Spikes by
698 Dynamic Time Warping and Affinity Propagation. Proc IEEE Int Conf Acoust Speech
699 Signal Process 2016; 2016: 749–753.

700 Tomlinson SB, Bermudez C, Conley C, Brown MW, Porter BE, Marsh ED.
701 Spatiotemporal Mapping of Interictal Spike Propagation: A Novel Methodology Applied
702 to Pediatric Intracranial EEG Recordings. Front Neurol 2016; 7: 1881.

703 Tse K, Puttachary S, Beamer E, Sills GJ, Thippeswamy T. Advantages of repeated low
704 dose against single high dose of kainate in C57BL/6J mouse model of status
705 epilepticus: behavioral and electroencephalographic studies. PLoS ONE 2014; 9:
706 e96622.

707 Twele F, Schidlitzki A, Töllner K, Löscher W. The intrahippocampal kainate mouse
708 model of mesial temporal lobe epilepsy: Lack of electrographic seizure-like events in
709 sham controls. Epilepsia Open 2017; 2: 180–187.

710 Twyman RE, Macdonald RL. Kinetic properties of the glycine receptor main- and sub-
711 conductance states of mouse spinal cord neurones in culture. J Physiol (Lond.) 1991;
712 435: 303–331.

713 Umpierre AD, Bennett IV, Nebeker LD, Newell TG, Tian BB, Thomson KE, et al.
714 Repeated low-dose kainate administration in C57BL/6J mice produces temporal lobe
715 epilepsy pathology but infrequent spontaneous seizures. Exp Neurol 2016; 279: 116–
716 126.

717 Wahlberg P, Lantz G. Methods for robust clustering of epileptic EEG spikes. IEEE Trans
718 Biomed Eng 2000; 47: 857–868.

719 Wallace E, Kim DY, Kim K-M, Chen S, Braden BB, Williams J, et al. Differential effects
720 of duration of sleep fragmentation on spatial learning and synaptic plasticity in pubertal
721 mice. Brain Res. 2015; 1615: 116–128.

722 Webber WR, Litt B, Lesser RP, Fisher RS, Bankman I. Automatic EEG spike detection:
723 what should the computer imitate? Electroencephalogr Clin Neurophysiol 1993; 87:
724 364–373.

725 Webber WRS, Lesser RP. Automated spike detection in EEG. Clin Neurophysiol 2017;
726 128: 241–242.

727 White A, Williams PA, Hellier JL, Clark S, Dudek FE, Staley KJ. EEG spike activity
728 precedes epilepsy after kainate-induced status epilepticus. Epilepsia 2010; 51: 371–
729 383.

730 Wilson SB, Emerson R. Spike detection: a review and comparison of algorithms. Clin
731 Neurophysiol 2002; 113: 1873–1881.